Bulletin of Electrical Engineering and Informatics
Vol. 15, No. 4, August 2026, pp. 3022∼3035
ISSN: 2302-9285, DOI: 10.11591/eei.v15i4.11329

Wideband bow-tie slot antenna with defected ground structure for efficient radio frequency energy harvesting

Usman Yau[1], Jun Jiat Tiang[1], Surajo Muhammad[2], Nazih Khaddaj Mallat[3], Isiyaku Yau[4]
[1]Centre for Wireless Technology, CoE for Intelligent Network, Faculty of Artificial Intelligence and Engineering, Multimedia University, Persiaran Multimedia, Cyberjaya, Malaysia
[2]Center for Intelligent Network Telekom Research and Development (TM R&D), Sdn Bhd, Multimedia University, Cyberjaya, Malaysia
[3]College of Engineering, Al Ain University, Al Ain, United Arab Emirates
[4]Department of Electronics and Telecommunications Engineering, Ahmadu Bello University, Zaria, Nigeria

Article Info

Article history:

Received Sep 3, 2025
Revised Jun 15, 2026
Accepted Jul 21, 2026

Keywords:

Bow-tie slot
Defected ground structure
Microstrip antenna
Power management module
Radio frequency energy harvesting
Wideband antenna

ABSTRACT

This work proposes the design and performance assessment of a wideband bow-tie slot antenna specifically developed for radio frequency energy harvesting (RFEH). The design employs a self-complementary bow-tie configuration, integrated with a defected ground structure (DGS) and fractal elements, to achieve improved bandwidth (BW) and gain. It achieved -10 dB simulated (measured) BW of 2.50 GHz (2.10 GHz) over a frequency span of 0.80-3.30 GHz (0.80 to 2.90 GHz) respectively. The results cover a target f_o, simulated and measured fractional bandwidth (FBW) of 122% and 114% respectively, with a peak realized gain of 6.42 dBi. The antenna also achieved a compact dimension of 126 mm × 90 mm (0.73 lambda g × 0.52 lambda g). It is finally integrated with a wideband RF-rectifier for the purpose of validation. The design enables continuous wireless power transfer (WPT) suitable for RFEH in internet of things (IoT) devices and sensor nodes.

Corresponding Author:

Jun Jiat Tiang
Centre for Wireless Technology, CoE for Intelligent Network, Faculty of Artificial Intelligence and Engineering
Multimedia University, Persiaran Multimedia
3100 Cyberjaya, Selangor, Malaysia
Email: jjtiang@mmu.edu.my

1. INTRODUCTION

The increasing demand for continuous power has led researchers into promising renewable energy technology. Abundant electromagnetic (EM) from various radio frequency (RF) sources can serve as additional source of energy [1], [2]. A rectenna is responsible for radio frequency energy harvesting (RFEH) [3]. The receiver is a vital component of wireless power transfer (WPT) technology that has undergone notable and sustainable advancements over the past few decades [4]–[6]. RFEH is viable for challenging applications, including health, environmental, defense monitoring, and fire detection [7]. A rectifying antenna is essential in WPTs, especially for internet of things (IoT) devices and sensor nodes, which depend on a reliable and secure power source [8]. The RF signals spans various frequencies within the microwave and industrial, scientific and medical (ISM) band. Frequencies include WLAN (2.40, 5.8 GHz), 0.9/1.8 GHz (GSM), Universal Mobile Telecommunication Service (UMTS) 2.10 GHz, and LTE 2.60 GHz. Various antennas operate across different frequency bands are discussed; however, the ambient RF power level typically remains between -40 and -50 dBm [9]–[14]. As 5G technology becomes more widely adopted, it is essential to consider the role of 5G as a significant power source. Deciding whether to exhibit broadband or multi-band characteristics is important when designing a receiving antenna. Therefore, it is necessary to develop an efficient RFEH system by creating a wideband or multi-band antenna with reasonable gain, bandwidth (BW) and an RF-rectifier with reduced circuit complexity. Patch antennas are frequently used in wireless communication systems due to their lightweight, affordability, and ease of fabrication [10], [15]. However, one of their limitations is narrow BW [16].

Various types of dual-band [16]–[19], triple-band [20]–[23], and multiband [24]–[27] designs have been presented for implementing RF harvesting in the microwave frequency range. Designing a wideband or multiband: (antenna with reasonable gain and BW), and (RF-rectifier with reduced circuit complexity) is needed for an efficient RFEH. To meet the demands of wideband systems, various techniques have been employed to enhance and broaden the BW of printed antennas and overcome this limitation. Broadband antenna designs have been presented, including the circular and elliptical disc monopoles [28], triangular [29], and planar volcano smoke slot antenna [30]. The dipole configuration's suitability in achieving the required characteristics for wideband applications has been studied using various shapes for the two arms, including circular, square, triangular, and others [31], [32]. A new category of printed antipodal drop shaped dipole antennas has been introduced for wireless communication systems [15]. The design have an operating BW exceeding 2 GHz, achieved through a well designed shaping of the feeding lines and radiating arms [33].

The bow-tie antenna is widely used in broadband applications, and improvements have been made to enhance its performance. One approach to improve its efficiency involved resistive loading, which enhances its radiation, minimizes late time ringing and reduces size [34]. A further enhancement was achieved by utilizing the Sierpinski fractal pattern on the bow-tie structure arms, generating multiple narrow operational frequency bands [35]. Several bow-tie antennas have been designed to ensure a decent impedance BW, generally within a 2 GHz range [36], [37]. Some of the designs also support a dual-band operation [38]. A specific frequency has been targeted for tuning similar design [39]. A four-bow-tie-element array was demonstrated using EM coupling microstrip patch antennas (ECMSAs); however, its BW was limited to 2.70-3.30 GHz [40]. A thorough review of bow-tie antenna literature shows that a suitable match between each side of the antenna and a practical feeding port, usually at 50 Ω, is a crucial challenge [41], [42]. Like biconical antennas, bow-tie antennas require a 300 Ω balanced transmission line for feeding [43].

The designer can choose between two methods to make the dipole compatible with a 50 Ω impedance. The first method involves using a balun transformer, which can be challenging to implement due to its limited BW and sometimes requires a complex shape and additional size [44], [45]. Alternatively, the second method involves using a multi-section line with varying widths or a gradually widened microstrip line to act as an impedance transformer, matching the bow tie to the Sub miniature version, A SMA connector [45], [46]. To enhance the antenna's performance, researchers have chosen to embed the bow-tie within a slot. This requires matching techniques, at least for the initial stage [47]. While some attempts have achieved matching across the entire BW of ultra-wideband (UWB), these solutions have made the design process more complex [34].

This study proposes a unique self-complementary bow-tie planar antenna (SCBPT) to address the challenges outlined. The design was able to achieve:
- Direct 50 Ω feed without an impedance transformer which eliminates complex impedance matching networks common in bow-tie designs, reducing fabrication complexity and minimizing insertion loss.
- Ultra-wide impedance fractional bandwidth (FBW) measured 114% (0.80–2.90 GHz), covering sub-GHz to mid-GHz bands relevant for RFEH.
- Compact electrical size of 0.73 $\lambda_g \times 0.52\ \lambda_g$ at f_o, significantly smaller than comparable state-of-the-art UWB bow-tie antennas.
- High realized gain of 6.42 dBi on FR-4 substrate.

2. WIDEBAND BOW-TIE-SLOT ANTENNA DESIGN AND ANALYSIS

This section describes the design of a proposed source antenna. A conventional bow-tie antennas are configured and fed through 300 Ω TL [48]–[50]. In this work, a unique bow-tie source antenna geometry is designed using a self-complementary technique [51]–[53]. The proposed design is fed through a 50 Ω SMA source without the use of impedance transformer. The geometry and optimized dimensions is depicted in Figure 1. The parameters in Figure 1 are optimized as: L_s=126, L_1=L_g=62, L_2=0.8, L_3=56.3, L_c=67.3, L_{c1}=64.8, L_f=60.2, L_h=0.6, L_j=2, L_t=61.6, W_s=90, W_1=53, W_2=15.4, W_3=1.6, W_4=16.0, W_c=60.2, W_g=26.8, W_h=17.2, W_j=21.0, and W_t=3.4 (all units are in mm). The design concept emanates from transforming a monopole triangular antenna radiator on LHS of the structure. A slot complement of the triangular radiator is added to RHS of the bottom plane. Microstrip feed line is bend to fed radiator at 50 Ω TL, as depicted in Ant-I of Figure 2.

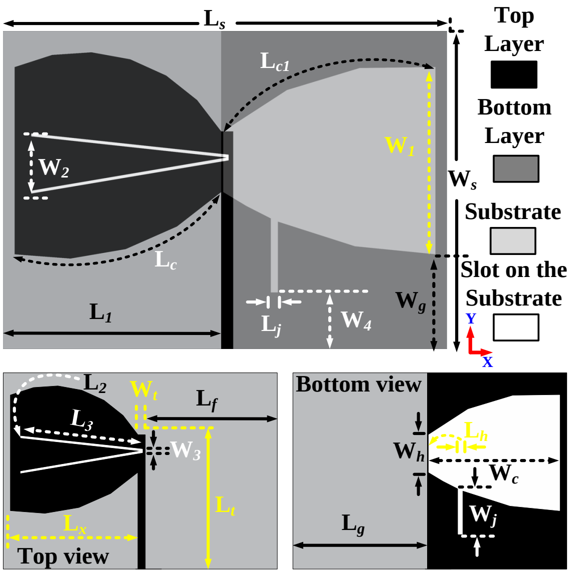

Figure 1. Top and bottom view of the proposed wideband bow-tie-slot antenna

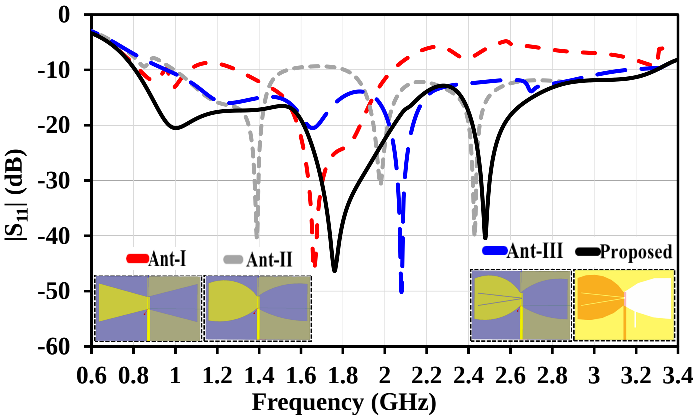

Figure 2. Design approach for optimizing the proposed bow-tie slot antenna

The lower frequency f_{l2} of the proposed design can be estimated using a relationship that is established by looking at the antenna as a monopole cylinder. The corresponding length is configured to match the patch length. Surface area of the cylinder is compared to that of the patch to determine it radius. A monopole triangular patch antenna is the closest shape to the Ant-I design structure, which is governed by the relation:

$$f_{l2} = \frac{7.2}{(L_x + R_t + P_g) \times m} GHz \tag{1}$$

where: all length dimensions L_x, R_t, and P_g are in cm, m is given by $\sqrt{\epsilon_{eff}}$, and ϵ_{eff} is the effective dielectric constant of the substrate.

L_x is the effective height of the monopole triangular patch. For an equilateral triangular patch with a base width W_1, L_x can be expressed as (2):

$$L_x = \frac{\sqrt{3}}{2} * W_1 \tag{2}$$

Since the height of an equilateral triangle is $\sqrt{3}/2$ times its base. Thus: $W_1 = 5.3\,\text{cm}$ (53 mm), it implies that; L_x=4.60 cm, The parameter R_t denotes the equivalent radius of a cylindrical monopole that exhibits EM characteristics comparable to those of a finite-width triangular patch. For a flat conductive plate of width W_1, a commonly used estimation of the equivalent radius is given by (3):

$$R_t = \frac{1}{4\pi} * W_1 \tag{3}$$

The triangular metal patch, having a base width W_1, can be modeled as an equivalent cylindrical wire of radius R_t. Substituting W_1=5.3 cm into the relation yields R_t=0.42 cm which is consistent with the design parameters employed in this work. The term R_t accounts for the combined effects of end fringing and capacitive loading caused by the radiator's finite width. This phenomenon leads wider elements to act similarly to thicker wires, which in turn produces a lower resonant frequency. The incorporation of fractal slots effectively increases the electrical length of the surface current paths, thereby generating additional higher order resonant modes. These modes interact with the fundamental resonance and collectively broaden the overall impedance BW. Furthermore, the fractal geometry facilitates smoother current distribution in vicinity of the feed region, which enhances impedance matching stability throughout the operating band. Defected ground structure (DGS), comprising three slits and a self complementary parasitic patch etched on the ground plane, modifies the surface current distribution and suppresses unwanted wave modes. This suppression effectively reduces the quality factor of the dominant resonant modes, resulting in a flattened response. Consequently, the radiation efficiency is enhanced, which contributes to the measured gain improvement within the mid frequency band.

In the context of this work, P_g refers to length of the feed probe or the gap, which defines spacing between the ground plane and the radiating element. For a microstrip-fed slot antenna, this dimension may indicate a small feed gap, or alternatively, the substrate thickness in cases where the feeding mechanism employs a coaxial probe. An increase in the feed probe or gap extends the effective length of the resonant structure, resulting in a reduction of the operating frequency. In the fabricated prototype, the parameter P_g is relatively small, approximately equal to the substrate thickness. A feed gap of P_g =0.06 cm (0.6 mm) was implemented, that is; L_h=P_g=0.6 mm.

The parameter ϵ_{eff} represents the effective dielectric constant experienced by the fields. For the bow-tie antenna fabricated on an FR-4 substrate (ϵ_r=4.7), the associated EM wave propagates within the dielectric medium and partly through air. That is:

$$\varepsilon_{\text{eff}} = \frac{\varepsilon_r + 1}{2} \tag{4}$$

Therefore; ε_{eff}=2.85. The effective permittivity appears in the expression as a multiplicative factor for the guided length, or equivalently as a divisor for the operating frequency, because wavelength within the substrate is shortened to:

$$\lambda_g = \frac{\lambda_0}{\sqrt{\varepsilon_{\text{eff}}}} \tag{5}$$

where λ_g denotes the guided wavelength and λ_0 represents the free-space wave length. A larger value of the effective permittivity, ε_{eff}, leads to a reduced wave velocity and a corresponding decrease in the resonant frequency for the same physical length. This behavior is incorporated in the expression for f_{l2} by placing ε_{eff} in the denominator. In a special case where $\varepsilon_{\text{eff}} = 1$ (air), the equation reduces to:

$$f_{l2} = \frac{7.2}{(L_x + R_t + P_g)} GHz \tag{6}$$

Based on (1), and considering the initial design parameters of W_1=5.3 cm, and the calculated values: L_x=4.60 cm, R_t=0.42 cm, and P_g=0.06 cm, with an effective permittivity of ε_{eff}=2.85. Therefore, the lower cutoff frequency is thus estimated as: f_{l2}=0.84 GHz.

This result closely matches the simulated and measured lower band edge of 0.80 GHz for the antenna, indicating that the formula provided a reliable initial basis for the design. The minor deviation observed is anticipated, as fine-tuning and factors such as inclusion of the ground slot and stubs can cause slight shifts in the resonant frequency.

By incorporating a bow-tie configuration together with additional features, including slot loading, multiple resonances are induced and subsequently merged, resulting in an UWB performance. The triangular patch by itself supports a fundamental resonance and possibly higher order modes. By integrating a fractal geometry and a DGS, additional resonant modes are excited, thereby enhancing coupling performance over an extended operational BW. The fractal slot length L_3 was tuned to approximately $56\,\mathrm{mm}$ to achieve precise control over the upper frequency band. Parametric results demonstrated that small adjustments in L_3 on the order of a few millimeters caused a distinct shift in the higher resonance, markedly affecting the high frequency S_{11} characteristics. By carefully optimizing the dimensional parameters, the proposed design attained an exceptionally wide FBW exceeding 110% defined as (7):

$$\mathrm{FBW} = \frac{f_{\max} - f_{\min}}{f_{\mathrm{center}}} \times 100\% \tag{7}$$

where $f_{\max}$ and $f_{\min}$ denote the upper and lower operating frequencies, respectively, and f_{center} is the center frequency.

For the proposed antenna, the lower cutoff frequency is approximately $f_{\min}$=0.80 GHz, while the upper cutoff frequency is $f_{\max}$=2.90 GHz. The mid-band center frequency can be taken as f_{center}=(f_{max}+f_{min})/2, therefore, f_{center}=1.85 GHz. Now, putting f_{center}=1.85 GHz in (7), it implies: FBW=114%.

A complement of the antenna triangular-slot is deployed in RHS of the bottom ground. To enhance the current flow and resonant modes, the radiator and it is ground complement are incorporated with two-semi circular slot to form a unique inverted-cone structure. This is depicted in Ant-II. To improved the lower resonant modes, the center radiator is then cut with two-slanted rectangular slit, as shown in Ant-III. This is then followed by the addition of rectangular slot to the lower arm of the ground plane for better matching to optimized the proposed design. Figure 2 provides the detailed approach of the source antenna. An inverted triangle or sloped radiator is used to fed the antenna through a 50 Ω TL.

Using detailed parametric analysis, the antenna designed in HFSS is then further tuned, optimized and the results were noted. This involved systematic variation of some critical geometrical parameters, L_3, L_f, and W_h. Figure 3 demonstrates the effect of varying the parameter L_3 from 54 mm to 56.3 mm on the antenna's reflection coefficient (S_{11}).

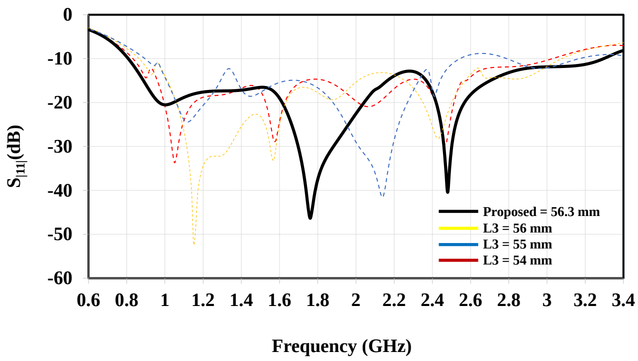

Figure 3. Parametric analysis of L_3

A gradual shift in resonance towards lower frequencies is observed as L_3 increases. Notably, the best impedance matching occurs at L_3=56 mm, where the antenna exhibits a wide -10 dB BW, covering approximately 0.8 GHz to 3.3 GHz. This shift in performance can be attributed to role of the ground stub, which alters the current distribution and effectively extends the electrical length of the radiating structure. L_f was systematically adjusted from 15.4 mm to 15.9 mm, as illustrated in Figure 4. The analysis reveals that a length of 15.7 mm achieves optimal impedance matching over the operating frequency band. Figure 5 illustrates the dependence of the peak realized gain on frequency for various values of W_h ranging from 16.9 mm to 17.2 mm. The highest gain performance is achieved at W_h=17.1 mm, where the antenna maintains a stable gain exceeding 3 dBi across the 1.8-2.8 GHz band. This improvement is primarily due to enhanced radiation efficiency and optimal mode excitation resulting from the fine-tuned slot width.

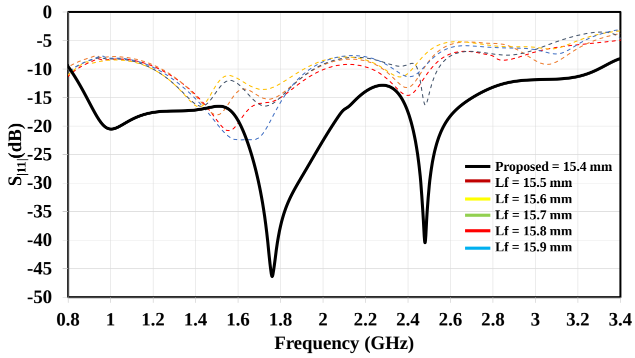

Figure 4. Parametric analysis of L_f

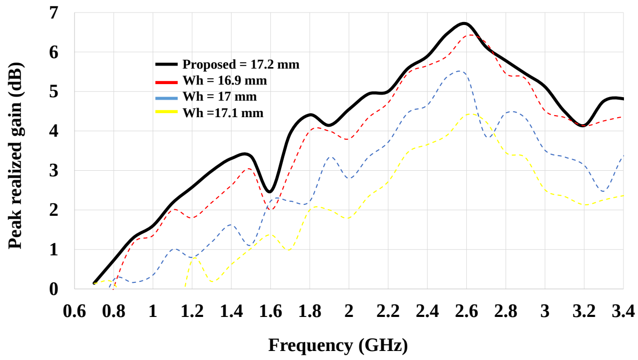

Figure 5. Parametric analysis of W_h

3. SIMULATED AND MEASURED RESULTS

The simulated (measured) $|S_{11}|$ as a function of frequency of the proposed wideband bow-tie-slot antenna is presented in Figure 6. The two results were acceptable within the context of the desired operating BW. The slight variation from the measured data is attributed to fabrication tolerance between the top and bottom view, SMA source or connection loss, and soldering lead loss.

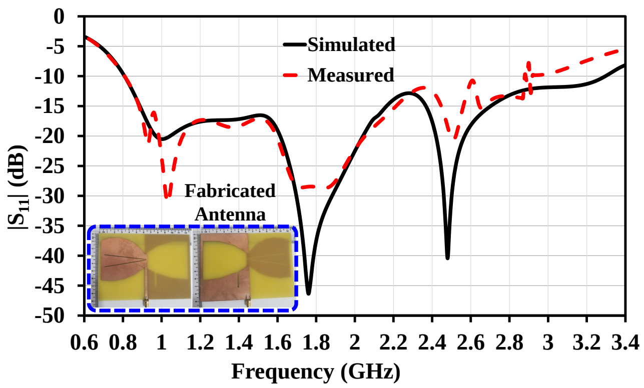

Figure 6. Simulated and measured: reflection coefficient ($|S_{11}|$)

The proposed design achieved -10 dB simulated and measured BW of 2.50 GHz over a frequency span of 0.80 to 3.30 GHz and 2.10 GHz between 0.80 to 2.90 GHz respectively. The results findings cover a target f_o, amounting to 122% and 114% of the simulated and measured FBW, respectively. The antenna's measured $|S_{11}|$ is in close agreement with the simulated data. The peak realized gain simulated (measured) achieved by the proposed bow-tie slot antenna is 6.71 dBi (6.42 dBi) at 2.60 GHz as depicted in Figure 7. The measured impedance BW is reported at 1.590 GHz between 1.550 and 3.140 GHz.

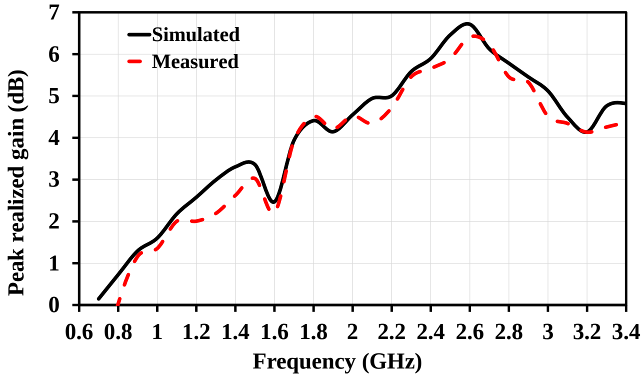

Figure 7. Simulated and measured: peak realized gain, of the bow-tie slot antenna as a function of frequency

To experimentally evaluate performance of the proposed design for RFEH, a complete rectenna system was constructed and tested under ambient conditions. As depicted in Figure 8, the measurement setup consisted of three main components: the bow-tie antenna, a rectifier circuit, and a power management module (PMM) connected at the output stage. The antenna was designed to function within the sub-GHz frequency spectrum, primarily targeting ambient RF signals radiated from proximal cellular base stations. Its structure was meticulously optimized to facilitate efficient harvesting of incident EM energy. In order to transform the received RF signals into usable DC output, the designed antenna was interfaced with a high-efficiency rectification circuit.

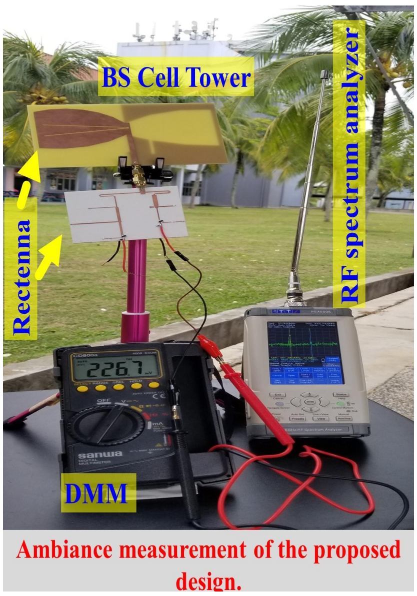

Figure 8. Experimental setup for validating the performance of the proposed bow-tie antenna integrated with a rectifier and PMM

The RF-rectifier, which has been rigorously tested and validated in earlier studies [54], offers low-loss performance and optimal compatibility with the antenna's operating bands. Architecture of the rectifier circuit layout is shown in Figure 9. By incorporating this rectifier into the system, it becomes possible to directly assess the real-time energy harvesting behavior of the antenna under practical environmental conditions.

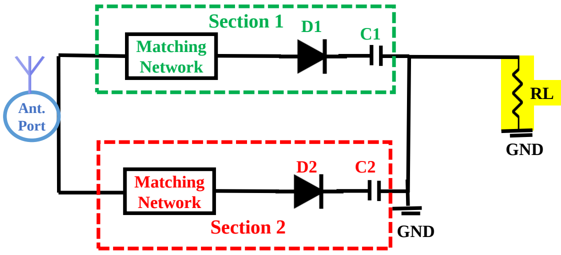

Figure 9. Integrated RF-rectifier circuit layout

To regulate and store the DC power harvested at the rectifier's output, a PMM was employed. It also ensures voltage stability and supports uninterrupted power supply to downstream IoT devices and sensor nodes. In addition, it provides an accurate mechanism for monitoring the extracted power, thereby allowing for a quantitative assessment of the system's energy harvesting performance. The ambient RF environment was assessed using a 6 GHz Aim spectrum analyzer (TTiPSA6005), which enabled real-time monitoring of the incident spectral content. A digital multimeter (DMM) was utilized concurrently to measure the DC output voltage generated. Under typical ambient conditions, the system delivered a V_{dc} of approximately 226.7 mV. By correlating the measured incident RF power with the corresponding V_{dc}, the RF-to-DC PCE was determined to be 27%. These findings validate the effectiveness of the integrated bow-tie antenna and rectifier system in harvesting ambient RF energy.

Figure 10(a) illustrates the simulated and measured radiation patterns at 0.9 GHz, where a quasi-omnidirectional distribution is observed in the H-plane, while the E-plane exhibits a characteristic dipole-shaped radiation profile. Such radiation behavior is consistent with the fundamental resonance of the proposed structure. The radiation performance of the antenna at 1.8 GHz is presented in Figure 10(b). This indicate that the antenna preserves a stable broadside radiation profile, while exhibiting moderate beam narrowing relative to its operation at 0.9 GHz. At 2.1 GHz, as illustrated in Figure 10(c), the radiation pattern exhibits a high degree of symmetry, with only slight deviations observed. The result showed that the incorporation of complementary slot and fractal structures preserves the antenna's radiation characteristics without introducing significant performance degradation. Figure 10(d) presents the radiation characteristics at 2.4 GHz. At this frequency, a higher radiation intensity is observed in the broadside direction, which is attributed to the improved EM coupling between the bow-tie radiator and the DGS. This enhanced interaction contributes to the increase in antenna gain, as demonstrated in Figure 7. Finally, Figure 10(e) presents patterns at 2.6 GHz, corresponding to the highest operating frequency within the investigated band. At this frequency, the proposed antenna achieves its maximum measured realized gain of approximately 6.42 dBi. The close correlation between the simulated and measured radiation characteristics confirms the consistency of the proposed self-complementary bow-tie configuration, demonstrating its ability to maintain stable radiation performance throughout the upper frequency region of the operating BW.

Figures 11(a)-(d) presents the surface current distribution, which provides a clear understanding of the EM behavior of the antenna throughout its operational BW. The current distributions were analyzed at 0.9 GHz, 1.8 GHz, 2.4 GHz, and 2.45 GHz to determine the dominant resonant mechanisms associated with each operating frequency. At 0.9 GHz, which lies near the lower edge of the operating band, the surface current distribution is primarily concentrated along the outer edges of the bow-tie arms and the lower portion of the radiator as shown in Figure 11(a). A pronounced current path is further observed extending toward the feeding region and propagating along the complementary slot etched in ground plane. The pattern confirms that, at the specified frequency, the antenna functions mainly in its fundamental monopole-type mode. The triangular radiator, together with the complementary slot introduced in the ground plane, extends the effective current path and thereby increases the electrical length of the structure. This mechanism enables the antenna to resonate in the sub-GHz region while preserving a reduced physical footprint. At 1.8 GHz, the surface current is more uniformly distributed along both arms of the bow-tie radiator as depicted in Figure 11(b).

A pronounced concentration of current is observed near the central feed point and along edges of the inclined rectangular slots. This behavior suggests the excitation of higher order resonant modes within the structure. The incorporation of fractal inspired slot features introduces supplementary current paths, which interact constructively with the fundamental resonant mode. As a result, the overall resonance is reinforced, leading to enhanced impedance matching across the mid band frequency region. Figures 11(c) and (d) illustrates the current distributions at 2.4 GHz and 2.45 GHz, the distributions becomes more concentrated along the inner edges of the bow-tie arms, the semi-circular slots, and the feed transition region. The elevated current density observed in these areas indicates enhanced EM coupling between the radiating element and the complementary ground structure. The current paths are observed to be shorter and more spatially confined than those at 0.9 GHz, which is characteristic of higher frequency operation. Furthermore, coupling between the slotted ground plane and the radiating arms promotes the excitation of multiple resonant modes that are closely spaced in frequency. The close proximity of the resonant modes leads to spectral overlap, which collectively produces the measured FBW of 114%. Furthermore, the symmetry evident in the current distribution at the mid and upper band frequencies aligns with the stable radiation patterns illustrated in Figures 10(a)-(e). The uniform distribution across the two arms reduces cross-polarization effects and preserves stable radiation performance in both the E and H-planes. As a result, the antenna exhibits a comparatively steady gain over the operating bands.

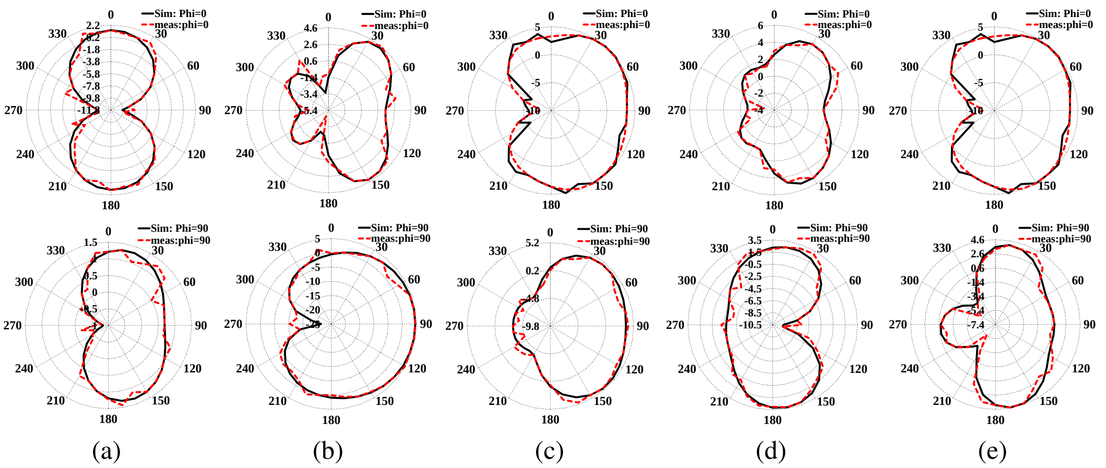

Figure 10. Measured and simulated radiation patterns of the antenna for phi=0^0 and phi=90^0: (a) at 0.9 GHz, (b) at 1.8 GHz, (c) at 2.1 GHz, (d) at 2.4 GHz, and (e) at 2.6 GHz

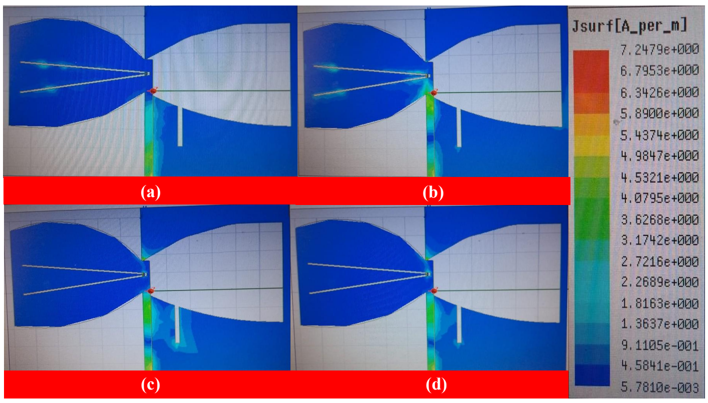

Figure 11. Current distribution plots of the antenna at: (a) 0.9 GHz, (b) 1.8 GHz, (c) 2.4 GHz, and (d) 2.45 GHz

4. COMPARATIVE ANALYSIS

A comparative analysis of the proposed bow-tie slot antenna and selected designs from existing literature is summarized in Table 1, highlighting key performance metrics. The developed antenna offers a wide operational BW ranging from 0.80 GHz to 2.90 GHz, which corresponds to a FBW of 114% and integrated rectifier PCE performance of 75%. Although this value is slightly lower than the maximum reported FBW of 118% in [55], the proposed design achieves this performance while maintaining a much smaller physical footprint. The antenna occupies a compact electrical area of 0.73×0.52, which is significantly smaller than the design reported in [55] (2.40×2.40) and [39] (2.26×0.51). Moreover, the antenna demonstrates an impressive peak gain of 6.42 dBi, exceeding the results of [15], [19], [34], [37], despite being implemented on a simpler and more affordable FR-4 substrate (ε_r=4.7). This performance underscores its ability to effectively balance compactness, gain, and BW, making it a promising solution for broadband energy harvesting and size-constrained.

Table 1. Performance evaluation of a proposed bow-tie slot antenna compared to reference results

Ref	Frequency (BW): GHz	FBW (%)	Size λ_g×λ_g	Peak gain (dBi)	Relative permittivity (ε_r)	Rectifier PCE (%)
[15]	2.375–2.65 (0.275)	11	0.83×0.83	1.8	NinjaFlex (3.0)	50
[19]	0.8–1.16 (0.36)	37	0.60×0.60	9	FR-4 (4.4)	65
[34]	1.41–1.86 (0.45)	27.50	0.35×0.35	1.31	FR-4 (4.4)	NA
[37]	2.00–2.7 (0.70)	28.50	0.67×0.67	2.49	Taconic (3.5)	NA
[39]	4.28–4.64 (0.36)/5.16–5.52 (0.36)	8.07/6.74	2.26×0.51	3.58	4D Nylon (3.1)	55
[47]	2.26–2.57 (0.31)/4.81–6.656 (1.76)	12.8/30.80	0.95×0.72	2.55/3.65	FR-4 (4.4)	50
[55]	2.75–10.70 (7.95)	118	2.40×2.40×0.40	10.8	F4B (2.65)	60
This work	0.80–2.90 (2.10)	114	0.73×0.52	6.42	FR-4 (4.7)	75

λ_g is wavelength at the lowest operating frequency (f_o) and NA is not applicable

5. CONCLUSION

This paper presents the design of a compact and high-efficiency wideband bow-tie slot antenna, specifically optimized for harvesting ambient RF energy. The antenna demonstrates enhanced impedance BW and gain through the integration of a self-complementary structure, fractal geometry, and DGS, thereby eliminating the reliance on complex IMN. By integrating semi-circular and slanted rectangular slots, the design achieves efficient multi-band resonance and a more uniform surface current distribution. Furthermore, the direct 50 Ω feeding mechanism reduces design complexity, thereby simplifying practical realization. The measured and simulated results demonstrate FBW of 114% and 122%, respectively, centered around the target frequency f_o. A peak realized gain of 6.42 dBi was recorded at 2.60 GHz. The antenna exhibits a compact form factor with overall dimensions of 126 mm × 90 mm, corresponding to 0.73 λ_g × 0.52 λ_g. To validate its practical application, the antenna was integrated with a wideband RF rectifier. Under typical ambient RF energy conditions, the integrated system produced a measurable DC output voltage and achieved a favorable PCE.

In addition, the proposed wideband bow-tie slot antenna presents strong prospects for real world integration within next generation IoT platforms and self-sustaining sensor network architectures. Due to its ultra wide FBW, stable gain characteristics, and direct 50Ω feed configuration, it efficiently captures heterogeneous ambient RF signals distributed across both sub-GHz and mid-GHz communication bands. This characteristic renders the proposed system particularly well suited for battery-less IoT nodes, distributed environmental monitoring platforms, and smart infrastructure deployments, where sustained, maintenance free operation over extended periods is a fundamental requirement. In these scenarios, dependable ambient energy harvesting can substantially reduce reliance on conventional battery based power supplies, thereby extending device operational lifetime, improving patient safety, and promoting overall system sustainability. Accordingly, the proposed architecture offers not only an efficient RFEH mechanism but also a viable framework for realizing self powered next generation wireless systems.

ACKNOWLEDGMENTS

The authors acknowledge the support of TM Research and Development (TM R&D) Malaysia for this work.

FUNDING INFORMATION

This work was financially supported by TM Research and Development (TM R&D) Malaysia under the Academic Co-Creation Project (Grant No. RDTC/241135: WBT-BIOM) and Project MMUE/240100.

AUTHOR CONTRIBUTIONS STATEMENT

This journal uses the Contributor Roles Taxonomy (CRediT) to recognize individual author contributions, reduce authorship disputes, and facilitate collaboration.

Name of Author	C	M	So	Va	Fo	I	R	D	O	E	Vi	Su	P	Fu
Usman Yau	✓	✓	✓	✓					✓	✓	✓			
Jun Jiat Tiang						✓				✓		✓	✓	
Surajo Muhammad	✓		✓			✓				✓		✓		
Nazih Khaddaj Mallat					✓		✓		✓					
Isiyaku Yau	✓							✓		✓		✓		

C	: **C**onceptualization	I	: **I**nvestigation	Vi	: **Vi**sualization
M	: **M**ethodology	R	: **R**esources	Su	: **Su**pervision
So	: **So**ftware	D	: **D**ata Curation	P	: **P**roject Administration
Va	: **Va**lidation	O	: Writing - **O**riginal Draft	Fu	: **Fu**nding Acquisition
Fo	: **Fo**rmal Analysis	E	: Writing - Review & **E**diting		

CONFLICT OF INTEREST STATEMENT

The authors declare no conflict of interest.

DATA AVAILABILITY

The data supporting the findings of this study are available within the article. Additional design files, measurement data, and supporting materials are available from the corresponding author, J.J.T., upon reasonable request.

REFERENCES

[1] S. K. Divakaran, D. D. Krishna, and Nasimuddin, "RF Energy Harvesting Systems: An Overview and Design Issues," *International Journal of RF and Microwave Computer-Aided Engineering*, vol. 29, no. 1, p. e21633, 2019, doi: 10.1002/mmce.21633.

[2] S. N. Arinze, E. R. Obi, S. H. Ebenuwa, and A. O. Nwajana, "RF Energy-Harvesting Techniques: Applications, Recent Developments, Challenges, and Future Opportunities," *Telecom*, vol. 6, no. 3, pp. 1-40, 2025, doi: 10.3390/telecom6030045.

[3] M. A. Halimi, T. Khan, A. A. Kishk, and Y. M. M. Antar, "Rectifier Circuits for RF Energy Harvesting and Wireless Power Transfer Applications: A Comprehensive Review Based on Operating Conditions," *IEEE Microwave Magazine*, vol. 24, no. 1, pp. 46–61, 2023, doi: 10.1109/MMM.2022.3211594.

[4] D. Sarkar, T. Khan, F. A. Talukdar, and S. R. Rengarajan, "Computational Intelligence for Modeling and Optimization of RFEH and WPT Systems: A Comprehensive Survey," *IEEE Microwave Magazine*, vol. 24, no. 9, pp. 46–60, 2023, doi: 10.1109/MMM.2023.3284764.

[5] J. Soleimani and G. K. Kurt, "High-Power Radio Frequency Wireless Energy Transfer System: Comprehensive Survey on Design Challenges," *IET Wireless Sensor Systems*, vol. 14, no. 6, pp. 248–264, 2024, doi: 10.1049/wss2.12089.

[6] L. Ramalingam *et al.*, "The Advancement of Radio Frequency Energy Harvesters (RFEHs) as a Revolutionary Approach for Solving Energy Crisis in Wireless Communication Devices: A Review," *IEEE Access*, vol. 9, pp. 106107–106139, 2021, doi: 10.1109/ACCESS.2021.309889.

[7] O. V. Ekunke *et al.*, "Innovations in Fire Detection and Suppression Systems for Oil Refinery Operations," *Path of Science*, vol. 10, no. 11, pp. 4001–4015, 2024, doi: 10.22178/pos.111-7.

[8] T. P. G. van Nunen, R. M. C. Mestrom, and H. J. Visser, "Wireless power transfer to biomedical implants using a class-E inverter and a Class-DE rectifier," *IEEE Journal of Electromagnetics, RF and Microwaves in Medicine and Biology*, vol. 7, no. 3, pp. 202-209, Sept. 2023, doi: 10.1109/JERM.2023.3267042.

[9] P. Zhang, H. Yi, H. Liu, H. Yang, G. Zhou, and L. Li, "Back-to-Back Microstrip Antenna Design for Broadband Wide-Angle RF Energy Harvesting and Dedicated Wireless Power Transfer," *IEEE Access*, vol. 8, pp. 126868-126875, 2020, doi: 10.1109/ACCESS.2020.3008551.

[10] R. Azim, M. T. Islam, H. Arshad, M. M. Alam, N. Sobahi, and A. I. Khan, "CPW-Fed Super-Wideband Antenna With Modified Vertical Bow-Tie-Shaped Patch for Wireless Sensor Networks," *IEEE Access*, vol. 9, pp. 5343-5353, 2021, doi: 10.1109/ACCESS.2020.3048052.

[11] B. Behera, S. Mishra, M. H. Alsharif, P. Uthansakul, and M. Uthansakul, "A metasurface-inspired printed monopole antenna for 5G and RF energy harvesting application," *Engineering Science and Technology, an International Journal*, vol. 51, p. 101638, 2024, doi: 10.1016/j.jestch.2024.101638.

[12] B. R. Dutta, R. Chaudhury, A. Tripathi, and B. Biswas, "Advance T-shaped Microstrip Patch Antenna for Improved Radio Frequency Energy Harvesting," *Telecommunications and Radio Engineering*, vol. 83, 2024, doi: 10.1615/TelecomRadEng.2023049976.

[13] G. Moloudian *et al.*, "RF Energy Harvesting Techniques for Battery-Less Wireless Sensing, Industry 4.0, and Internet of Things: A Review," *IEEE Sensors Journal*, vol. 24, no. 5, pp. 5732-5745, 2024, doi: 10.1109/JSEN.2024.3352402.

[14] M. C. Derbal and M. Nedil, "High-Gain Circularly Polarized Antenna Array for Full Incident Angle Coverage in RF Energy Harvesting," *IEEE Access*, vol. 11, pp. 28199-28207, 2023, doi: 10.1109/ACCESS.2023.3259429.

[15] J. Li, Y. Jiang, and X. Zhao, "Circularly Polarized Wearable Antenna Based on NinjaFlex-Embedded Conductive Fabric," *International Journal of Antennas and Propagation*, vol. 2019, no. 1, 2019, doi: 10.1155/2019/3059480.

[16] K. Çelik, E. Kurt, and O. Korkmaz, "A Novel Multiple-Slot Pixel Patch Antenna for Wideband Terahertz Applications," *JOM*, vol. 77, no. 5, pp. 2967–2975, 2025, doi: 10.1007/s11837-024-07039-7.

[17] J. Zhao, J. Song, D.-a. Li, Y. Li, and J. Cheng, "Dual-band RF energy harvesting for low-power IoT devices," *Wireless Networks*, vol. 30, pp. 2511–2527, 2024, doi: 10.1007/s11276-024-03685-6.

[18] G. A. Baky *et al.*, "CPW-Fed Bow-Tie Antenna for Ambient RF Energy Harvesting Applications," in *2023 5th Novel Intelligent and Leading Emerging Sciences Conference (NILES)*, Giza, Egypt, 2023, pp. 416-419, doi: 10.1109/NILES59815.2023.10296596.

[19] A. Darvazehban, S. A. Rezaeieh, and A. Abbosh, "Wideband Beam-Switched Bow-Tie Antenna With Inductive Reflector," *IEEE Antennas and Wireless Propagation Letters*, vol. 19, no. 10, pp. 1724–1728, 2020, doi: 10.1109/LAWP.2020.3015512.

[20] D. Surender, Md. A. Halimi, T. Khan, F. A. Talukdar, and Y. M. M. Antar, "A triple band rectenna for RF energy harvesting in smart city applications," *International Journal of Electronics*, vol. 110, no. 5, pp. 789–803, 2023, doi: 10.1080/00207217.2022.2062797.

[21] A. Bakytbekov, T. Q. Nguyen, G. Zhang, M. S. Strano, K. N. Salama, and A. Shamim, "Dual-function triple-band heatsink antenna for ambient RF and thermal energy harvesting," *IEEE Open Journal of Antennas and Propagation*, vol. 3, pp. 263–273, 2022, doi: 10.1109/OJAP.2022.3149392.

[22] M. Aboualalaa, I. Mansour, and R. K. Pokharel, "Energy harvesting rectenna using high-gain triple-band antenna for powering internet-of-things (IoT) devices in a smart office," *IEEE Transactions on Instrumentation and Measurement*, vol. 72, pp. 1–12, 2023, doi: 10.1109/TIM.2023.3238050.

[23] M. A. Shukoor, V. Kumar, and S. Dey, "Compact polarisation insensitive wide angular stable triple band absorber for RF energy harvesting, RCS reduction, and sensor applications," *International Journal of RF and Microwave Computer-Aided Engineering*, vol. 31, no. 9, p. e22763, 2021, doi: 10.1002/mmce.22763.

[24] H. S. Vu, N. Nguyen, N. Ha-Van, C. Seo, and M. T. Le, "Multiband ambient RF energy harvesting for autonomous IoT devices," *IEEE Microwave and Wireless Components Letters*, vol. 30, no. 12, pp. 1189–1192, 2020, doi: 10.1109/LMWC.2020.3029869.

[25] M. A. Ullah, R. Keshavarz, M. Abolhasan, J. Lipman, K. P. Esselle, and N. Shariati, "A review on antenna technologies for ambient RF energy harvesting and wireless power transfer: Designs, challenges and applications," *IEEE Access*, vol. 10, pp. 17231–17267, 2022, doi: 10.1109/ACCESS.2022.3149276.

[26] D. N. Elshaekh, H. A. Mohamed, L. Y. A. El Menam, K. A. Sharshar, and S. I. Kayed, "Multiband printed rectenna for radio frequency energy harvesting (RF-EH)," *Discover Electronics*, vol. 2, no. 1, 2025, doi: 10.1007/s44291-025-00082-x.

[27] J. Sang *et al.*, "A triple-band and high-gain circularly polarized rectenna for radio-frequency energy harvesting applications," *IEEE Transactions on Antennas and Propagation*, vol. 73, no. 8, pp. 5223-5238, Aug. 2025, doi: 10.1109/TAP.2025.3564712.

[28] A. Wajid, M. I. Khan, M. Anab, and M. I. Khattak, "Design of Half Circular Disc Printed Monopole Antenna for Ultra Wide Band and Super Wide Band Applications," *Journal of Information Communication Technologies and Robotic Applications*, pp. 30–36, 2020, doi: 10.51239/jictra.v0i0.231.

[29] N. Nurhayati, T. Rijanto, P. W. Rusimamto, A. Abimanyu, S. P. J. Christydass, and A. Paleologoudias, "Impedance Bandwidth Enhancement of Monopole Antenna with Triangle Slot in the Ground Plane and Modified Patch for UWB Applications," in *2021 3rd International Conference on Research and Academic Community Services (ICRACOS)*, Surabaya, Indonesia, 2021, pp. 301-304, doi: 10.1109/ICRACOS53680.2021.9702006.

[30] J. Yeo, Y. Lee, and R. Mittra, "Wideband slot antennas for wireless communications," *IEE Proceedings–Microwaves, Antennas and Propagation*, vol. 151, no. 4, pp. 351–355, 2004, doi: 10.1049/ip-map:20040627.

[31] Z. Wu, X. Li, and X. Song, "An Improved Ultra-Wideband Circularly Polarized Cross-Dipole Antenna," in *2021 13th International Symposium on Antennas, Propagation and EM Theory (ISAPE)*, 2021, pp. 1-3, doi: 10.1109/ISAPE54070.2021.9752860.

[32] R. P. Dwivedi, M. Z. Khan, and U. K. Kommuri, "UWB circular cross slot AMC design for radiation improvement of UWB antenna," *AEU–International Journal of Electronics and Communications*, vol. 117, p. 153092, 2020, doi: 10.1016/j.aeue.2020.153092.

[33] R. Cicchetti, V. Cicchetti, A. Faraone, L. Foged, and O. Testa, "A compact high-gain wideband lens Vivaldi antenna for wireless communications and through-the-wall imaging," *IEEE Transactions on Antennas and Propagation*, vol. 69, no. 6, pp. 3177–3192, 2021, doi: 10.1109/TAP.2020.3037777.

[34] U. Khayam, A. A. Suryandi, and Rachmawati, "Design of Bowtie Antenna With Rounded Edge and Middle-Sliced Modifications for UHF Partial Discharge Sensor," *IEEE Access*, vol. 11, pp. 22822–22834, 2023, doi: 10.1109/ACCESS.2023.3252006.

[35] D. Tiwari, J. A. Ansari, A. K. Saroj, and M. Kumar, "Analysis of a Miniaturized Hexagonal Sierpinski Gasket Fractal Microstrip Antenna for Modern Wireless Communications," *AEU–International Journal of Electronics and Communications*, vol. 123, 2020.

[36] P. Li, J. Liang, Y. He, and H. Sun, "Dual-Polarized Low-Profile Millimeter-Wave Slot Antenna Array Using Substrate-Integrated Coaxial Line for Vehicular Wireless Applications," *IEEE Transactions on Vehicular Technology*, vol. 74, no. 12, pp. 18792-18802, Dec. 2025, doi: 10.1109/TVT.2025.3585645.

[37] A. Venouil, M. Egels, M. Benwadih, C. Serbutoviez, and P. Pannier, "Design Guidance of a Circularly Polarized Bowtie Antenna for ISM Bands," *Microwave and Optical Technology Letters*, vol. 65, no. 11, pp. 2972–2978, 2023, doi: 10.1002/mop.33812.

[38] A. Mehdipour, C. W. Trueman, A. R. Sebak, and S. V. Hoa, "Carbon-fiber composite T-match folded bow-tie antenna for RFID applications," in *2009 IEEE Antennas and Propagation Society International Symposium*, North Charleston, SC, USA, 2009, pp. 1-4, doi: 10.1109/APS.2009.5171640.

[39] L. Wu *et al.*, "Deformable Bowtie Antenna Realized by 4D Printing," *Electronics*, vol. 10, no. 15, pp. 1-9, 2021, doi: 10.3390/electronics10151792.

[40] P. Tiwari *et al.*, "A High Isolated, High Gain Millimeter Wave Quad-Port MIMO Antenna Array for Wideband 5G New Radio Application," *Scientific Reports*, vol. 15, no. 1, p. 34484, 2025, doi: 10.1038/s41598-025-18805-1.

[41] B. Maity and S. K. Nayak, "Compact Bowtie-Shaped Microstrip Patch Antennas With Low Cross-Polarization and Wideband Harmonic Suppression," *AEU–International Journal of Electronics and Communications*, vol. 168, p. 154699, 2023, doi: 10.1016/j.aeue.2023.154699.

[42] R. L. Yadava, *Antennas and Wave Propagation*. New Delhi: PHI Learning Pvt. Ltd., 2022.

[43] F. Zhang, F.-S. Zhang, Y.-B. Yang, and Z. Zhang, "Wide Band Antenna Array Using Bowtie-Shaped Microstrip Patch Antenna," in *2010 International Conference on Microwave and Millimeter Wave Technology*, Chengdu, China, 2010, pp. 424-427, doi: 10.1109/ICMMT.2010.5524993.
[44] G. Kumar, P. Mevada, S. Chakrabarty, and M. B. Mahajan, "Ultrawide Band Cage Dipole Antenna for Ultra High Frequency Band Ground Penetrating Radar System," *International Journal of RF and Microwave Computer-Aided Engineering*, vol. 32, no. 6, p. e23139, 2022, doi: 10.1002/mmce.23139.
[45] H. Koo and S. Nam, "Ku-Band Printed Bow-Tie Antenna H-Plane Array With Low Mutual Coupling," *IEEE Transactions on Antennas and Propagation*, vol. 72, no. 1, pp. 980-985, Jan. 2024, doi: 10.1109/TAP.2023.3336968.
[46] P. Gupta, R. U. Nair, and B. Choudhury, "Design of Stepped Bow Tie Antenna for Ultrawideband Applications," in *2022 IEEE 19th India Council International Conference (INDICON)*, Kochi, India, 2022, pp. 1-3, doi: 10.1109/INDICON56171.2022.10040200.
[47] L.-C. Tsai, "A Triple-Band Bow-Tie-Shaped CPW-Fed Slot Antenna for WLAN Applications," *Progress In Electromagnetics Research C*, vol. 47, pp. 167–171, 2014, doi: 10.2528/PIERC14011002.
[48] R. G. L. de Mello, A. C. Lepage, and X. Begaud, "The bow-tie antenna: Performance limitations and improvements," *IET Microwaves, Antennas & Propagation*, vol. 16, no. 5, pp. 283–294, 2022, doi: 10.1049/mia2.12242.
[49] H. Wang, Y. Feng, F. Hu, and Y.-X. Guo, "A Wideband Dual-Polarized Ring-Loaded Cross Bowtie Antenna for Wireless Capsule Endoscopes: Design and Link Analysis," *IEEE Transactions on Antennas and Propagation*, vol. 70, no. 9, pp. 7843-7852, Sept. 2022, doi: 10.1109/TAP.2022.3168272.
[50] Y.-Y. Jeong and W.-S. Lee, "Wideband Printed Half Bow-Tie Antenna Array Based on a Quad-Mode Reconfigurable Feeding Network for UAV Communications," *IEEE Open Journal of Antennas and Propagation*, vol. 2, pp. 238–248, 2021, doi: 10.1109/OJAP.2021.3057067.
[51] M. Alibakhshikenari *et al.*, "Dual-Polarized Highly Folded Bowtie Antenna with Slotted Self-Grounded Structure for Sub-6 GHz 5G Applications," *IEEE Transactions on Antennas and Propagation*, vol. 70, no. 4, pp. 3028-3033, Apr. 2022, doi: 10.1109/TAP.2021.3118784.
[52] Y. Li and J. Chen, "Design of Miniaturized High Gain Bow-Tie Antenna," *IEEE Transactions on Antennas and Propagation*, vol. 70, no. 1, pp. 738-743, Jan. 2022, doi: 10.1109/TAP.2021.3098595.
[53] A. A. Lestari, L. Simbolon, R. O. Bura, O. D. Winarko, and B. K. Pradekso, "UWB Wire-Bowtie Array for FM-PCL Passive Radar," *IEEE Transactions on Antennas and Propagation*, vol. 70, no. 9, pp. 7999-8007, Sept. 2022, doi: 10.1109/TAP.2022.3164920.
[54] S. Muhammad *et al.*, "Wideband RF Rectifier Circuit for Low-Powered IoT Wireless Sensor Nodes," *AEU–International Journal of Electronics and Communications*, vol. 170, p. 154787, 2023, doi: 10.1016/j.aeue.2023.154787.
[55] Z.-Y. Zhang, S. Zuo, X. Zhang, and G. Fu, "Ultra-Wideband Cavity-Backed Bowtie Antenna for Pattern Improvement," *Progress In Electromagnetics Research Letters*, vol. 37, pp. 37–46, 2013, doi: 10.2528/PIERL12110909.

BIOGRAPHIES OF AUTHORS

Usman Yau received the B.Eng. and M.Sc. degree in Electrical and Telecommunications Engineering from Ahmadu Bello University, Zaria, Nigeria, in 2019 and 2024 respectively. He is currently pursuing the Ph.D. degree in Wireless Power Transfer System (WPTs) for Biomedical Implants from Multimedia University (MMU), Cyberjaya, Selangor, Malaysia. His research interests include wireless power transfer systems for medical devices, RF energy harvesting for biomedical implants, 5G millimetre-wave antennas, and the design of wearable and implantable antennas. He has received TM R&D scholarship for his Ph.D. research. He can be contacted at email: usmanyau7@gmail.com.

Jun Jiat Tiang received the degree in electronics engineering from Multimedia University, Malaysia, the master's degree from the University of Science, Malaysia, and the Ph.D. degree from Universiti Kebangsaan Malaysia (UKM). He worked as a Design Automation Engineer with the Chipset Structural Design Team, Intel Microelectronics (M) Sdn. Bhd., Penang, Malaysia, from September 2004 to July 2005, and an Electronics Engineer with the Global Technology Development Group, Motorola Technology Sdn. Bhd., Penang, from May 2006 to May 2007. He has vast experience while working as the Project Leader in various research grants, such as TM Research and Development, from 2017 to 2020; Research Grant, Ministry of Science, Technology and Innovation (MOSTI), from 2008 to 2010; and research grant Mini Fund, in 2016. He is currently an Assistant Professor and a Researcher with the Faculty of Engineering, Multimedia University. His research interests include RFID, microwave circuits, antenna, and propagation. He was awarded the Gold Medal at the 23rd International Invention, Innovation, and Technology Exhibition (ITEX) 2012, Kuala Lumpur, Malaysia, in May 2012, and the Silver Medal at the Malaysian Technology Expo (MTE) 2013, Kuala Lumpur, in February 2013. He can be contacted at email: jjtiang@mmu.edu.my.

Dr. Surajo Muhammad earned his Bachelor of Engineering in Computer Engineering from Bayero University, Kano, Nigeria, in 2004. He completed a Master of Engineering in Electronics and Telecommunications Engineering at Universiti Teknologi Malaysia (UTM), Johor, Malaysia, in 2014, supported by the Kano State Government Overseas Scholarship. He then pursued his Ph.D. at Multimedia University (MMU) in Cyberjaya, Selangor, Malaysia, graduating in 2022. His doctoral studies were funded by a research grant from TM R&D Telekom Malaysia Berhad, where he served as a research scholar. In 2023, he expanded his expertise as a Postdoctoral Research Fellow with the Center for Wireless Technology (CWT) at MMU. His research interests include RF energy harvesting (RFEH) for biomedical implants, wireless power transfer systems for biomedical devices, 5G mm-wave antennas, and wearable and implantable antennas. He currently serves as a researcher at Telekom Research & Development (TM R&D) within the TM Innovation Centre in Cyberjaya, Selangor, Malaysia. He can be contacted at email: doguwa_2002@yahoo.com.

Dr. Nazih Khaddaj Mallat (Senior Member, IEEE) received his Bachelor's degree in Electrical and Electronics Engineering from Lebanese University, Lebanon, in 2000. He went on to earn a Master's degree in Information Technology from IMT Atlantique, France, in 2002, and a Ph.D. in Telecommunications from the University of Quebec, Canada, in 2010. After completing his Ph.D., he served as a Postdoctoral Fellow at École Polytechnique de Montréal until January 2012. In 2013, he joined the College of Engineering at Al Ain University (AAU) in the United Arab Emirates as an Assistant Professor and was promoted to Associate Professor in 2019. At AAU, he held multiple leadership positions: Head of the Networks and Communication Engineering and Computer Engineering Department from 2013 to 2017, Deputy Dean of the College of Engineering from 2014 to 2015, Dean of the College of Engineering from 2015 to 2018, and Director of the Quality Assurance and Institutional Research Center from 2018 to 2020. Since November 2020, he has served as the Vice President of Accreditation and Quality Assurance. He has gained extensive teaching experience at both undergraduate and graduate levels. He has taught numerous courses, along with their laboratory components, at several universities in Montreal, including ETS, TELUQ, and École Polytechnique de Montréal. His primary research interests encompass passive microwave and millimeter-wave circuits, antennas, and filters, and he has authored or coauthored over 60 publications in these areas. He is a member of the Ordre des Ingénieurs du Québec, Canada, and the Order of Engineers and Architects Tripoli, Lebanon. The Fonds Québécois de la Recherche sur la Nature et les Technologies (FQRNT), a Quebec government granting agency, awarded him two prestigious scholarships for his doctoral studies in 2008 and a postdoctoral research grant from 2010 to 2011 in recognition of his exceptional academic achievements. He is also the founder of the IEEE AAU Student Branch and the IEEE UAE MTT-S Chapter (which later became the IEEE UAE MTT-S, IM-S, and AP-S Joint Chapter). Previously, he served as Vice-Chair of the IEEE Montreal Section from 2007 to 2008, Membership Development Chair from 2009 to 2010, and Section Chair from 2011 to 2012. He has been actively involved in the steering committees of various IEEE international conferences and served as IEEE UAE Technical Activities Coordinator from 2015 to 2018, as well as IEEE Region 8 Chapter Coordination Subcommittee Chair in 2015 and 2016. He also chaired the organizing committees for three major events hosted by Al Ain University: the 1st IEEE International Workshop at AAU in February 2014, the 11th IEEE UAE Student Day in May 2016, and the 16th Mediterranean Microwave Symposium (MMS2016) in November 2016. He can be contacted at email: nazih.mallat@aau.ac.ae.

Isiyaku Yau is a Senior Lecturer in the Department of Electronics and Telecommunications Engineering of Ahmadu Bello University, Zaria. He received his B.Eng. degree in Electrical Engineering from Ahmadu Bello University, Zaria in the year 2012. He then received an M.Sc. and Ph.D. degrees in 2017 and 2022 respectively from the same University. He is actively involved in research activities and in fact a member of a team that worked on a research grant secured from the Nigerian Communications Commission (NCC) from the year 2018 to 2021. His research interests are mainly in optical communications, optical-wireless integration, RF system design, and wireless mobile communications. He can be contacted at email: isiyakuyau@abu.edu.ng.